Single-cell bacterium identification with a SOI optical microcavity

M. Tardif, J.-B. Jager, P. R Marcoux, K. Uchiyamada, E. Picard, E. Hadji, D. Peyrade

This manuscript was accepted by Appl. Phys. Lett. Click here to see the version of record.

Single-cell bacterium identification with a SOI optical microcavity

M. Tardif[1,2,*] , *J-B Jager*[2], *P.R. Marcoux*[3] , *K. Uchiyamada*[4], *E. Picard*[2], *E.Hadji*[2] , *D. Peyrade*[1,†]

[*] Electronic mail: manon.tardif@cea.fr

[†] Electronic mail: david.peyrade@cea.fr

[1] Univ. Grenoble Alpes, CNRS, LTM - Micro & Nanotechnologies for Health, 38054 Grenoble Cedex 9, France

[2] CEA & Univ. Grenoble Alpes, INAC-SP2M-SINAPS, 38000 Grenoble, France

[3] CEA, LETI-DTBS-SBSC-LCMI/LBAM, 38054 Grenoble Cedex 9, France

[4] Graduate School of Pure and Applied Sciences, University of Tsukuba, 1-1-1 Tennodai, Tsukuba, Ibaraki 305-8573, Japan

Abstract

Photonic crystals and microcavities act as on-chip nano-optical tweezers for identification and manipulation of biological objects. Until now, optical trapping of virus and bacteria has been achieved and their presence in the vicinity of the optical resonator is deduced by the shift in the resonant wavelength. Here, we show trapping and identification of bacteria through a properly tuned silicon on insulator microcavity. Through the spatial and temporal observations of bacteria–cavity interaction, the optical identification of three different kinds of bacteria is demonstrated.

This manuscript was accepted by Appl. Phys. Lett. Click here to see the version of record.

Biological objects are strategic components for medical and pharmaceutical development, faster clinical diagnosis and food processing control. The field of photonics has proven to be extremely suitable for the study of such objects. The first tool that allowed their trapping and manipulation is optical tweezers[1,2] which is based on the concentration of laser beam through a microscope objective. Unfortunately, this method is limited by the macroscopic scale of the implementation set-up and, especially, by the damage caused to cells[3,4] and bacteria[5–7] during optical manipulation. On the contrary, the evanescent field of on-chip optical resonators offers low light intensity that minimizes biological object damage. Therefore, they are more suitable for biomolecules,[8–12] viruses[13,14] and bacteria[15,16] manipulation at a microscopic scale.

For the past 20 years, many designs of optical resonators have emerged. From the 1D[17–19] and 2D[20–22] photonic crystals (PhC) to toroid,[23–25] ring,[26] cylindrical[27] and microspherical[28,29] resonators, extremely narrow resonances and quality factors as high as 10^9 have been achieved. With their integration in optofluidic devices, these structures allow micro and nano object manipulation[30–36] and biological object detection.[37,38] More specifically, at the cell scale, despite the low index contrast with liquid medium, it has been proven that bacteria trapping is achievable on PhC microcavities.[15] For these structures, the trap stiffness was quantified and the confined Brownian motion of bacteria has revealed dependence on light power excitation.[15] Thus, according to recent advancements, photonic crystal cavities appear to be suitable tools for bacteria manipulation.

Most of the work has been focused on detection where the high quality factor structures are required to precisely detect the shift in the resonance wavelength which is due to the refractive index variation near the resonator[12,37,38] (Figure 1(a)). Here we introduce the use of a broader resonance that is adapted for single bacterium analysis and label-free identification (Figure 1(b)). In order to achieve this condition, the resonance must be wide enough to allow

This manuscript was accepted by Appl. Phys. Lett. Click here to see the version of record.

an overlap between the resonance without bacterium and the resonance when the bacterium interacts with the field in the cavity (redshift).

Henceforth, we investigate an optical method based on microcavities to perform single-cell characterization of bacteria. The analysis of the cell's Brownian motion in the trap combined with the transmission signal from the optical structure allows a fine characterization of the cell behavior. Moreover, by analyzing the fluctuations in the transmitted signal over time during bacteria trapping, we observe variations between bacteria phenotypes.

A 1D microcavity resonator is made on SOI substrate (250 nm / 2 µm / 700 µm) by combining electron beam lithography and reactive-ion etching. The two mirrors are designed for mode adaptation within the cavity[39] (Figure 2(a)) in order to get a quality factor of 4000. In this study we used the same optical structure for all the experiments. By injecting the resonance wavelength in this structure (laser at λ_{res} = 1.5 µm, injected power P_{inj} = 10 mW, and linewidth L_w = 150 kHz), an intense and confined electromagnetic field is built in the cavity. The evanescent part of this field above the cavity creates optical gradient forces capable of trapping and manipulating colloidal objects.

Above the optical structures, a PDMS fluidic system leads colloids to the evanescent field. It consists a 100 µm thick PDMS film with molded microfluidic channel in which a drop of water/bacteria solution is present. It is then covered with a 150 µm thick layer of glass. This optofluidic chip is shown in Figure 2(b). A polarization-maintaining fiber enables the optical coupling of light from a tunable laser in the microcavity. Two microscope objectives are placed on-top and in-line with the chip and connected to the detection devices, which allows spatial

(images) and temporal (signal) characterization of the trapping. Images of the cavity are taken by microscope connected to a CCD camera, with a time resolution of 1/24s. To track bacteria

This manuscript was accepted by Appl. Phys. Lett. Click here to see the version of record.

trajectories, their position was detected on every recorded image for a relevant duration (few seconds), using tracking macro of Fiji (image processing package of ImageJ).[40] This analysis is shown in Figure 2(b-SPATIAL).

The signal transmitted by the optical structure is detected by a photodiode, increased by a transimpedance amplifier and displayed on an oscilloscope. The oscillations observed Figure 2(bTEMPORAL) are due to the shift in the resonance wavelength of the optical structure in the presence of bacterium above the cavity. In fact, the resonance wavelength does not depend only on the optical index of the cavity, but also on the index of the environment. When the bacterium interacts with the electromagnetic field in the cavity, the environmental index ranges from n_{water} = 1.33 (bacterium outside the cavity, only water above it) to 1.368 < $n_{bacterium}$ < 1.413 (bacterium exactly above the cavity).[41] This phenomenon is shown in Figure 1: it induces a less than 1 nm shift in the resonance wavelength, from the grey to the blue curve. As we keep injecting the same wavelength during all trapping experiments (resonance at n_{water}), the signal oscillates between the two intensity values IMIN and IMAX while the bacterium oscillates between two positions: trapped above and free around the cavity.
With this method, we are able to record simultaneously the position of the trapped object and the fluctuation in the transmitted signal.

The objects under study are the following bacteria, shown in Figure 2(c): *Staphylococcus epidermidis* (aggregated as *diplococcus*), *Escherichia coli* and *Bacillus subtilis* aggregate. They were selected because of their similar size to the previously studied polystyrene beads[31,42,43] and the differences in morphology and Gram-type between them. Gram staining is the most widely employed staining method in diagnostic bacteriology[44]. It divides bacteria into two major groups, gram-positive and gram-negative, based on their response to the

This manuscript was accepted by Appl. Phys. Lett. Click here to see the version of record.

Gram-stain procedure. These two groups correspond to structural differences in the cell wall. *B. subtilis* is a Gram+ *bacillus*, *E. coli* a Gram- *bacillus* and *S. epidermidis* a Gram+ *coccus*. *Diplococci* arise when *cocci* divide and remain together to form pairs. An *E. coli* cell and a *diplococcus* of S. *epidermidis* have equivalent size and shape: oval shape and size of 1 µm x 2 µm, compared to a more elongated shape of 1 µm x 7 µm for *B. subtilis* (aggregate). *E. coli* and *B. subtilis* have flagella, a molecular motor which enables them to swim in an aqueous medium. Bacterial strains (*E. coli* ATCC 117775, *S. epidermidis* ATCC 14990, *B. subtilis* ATCC 11774) were obtained from KwikStik lyophilized reference strains (Microbiologics, St. Cloud, MN). Starting with a culture of agar media (COS or TSA, bioMérieux) after 24h of incubation (37°C), a 0.5 McF suspension (Densimat, bioMérieux) was prepared in API Suspension medium (bioMérieux).

Following are the two analysis methods for understanding and characterizing bacteria trapping.

The Brownian motion of each type of studied bacterium and the effect of trapping on their trajectory is shown in Figure 3. We characterize the effect of the trap by a parameter called "confinement factor" which is the ratio of the rectangular area covered by bacteria position (L x l) without and with trapping. The trapping is demonstrated by the reduction in the displacement area (confinement factors between 3.2 and 57) and its major effect is a transversal confinement (area reduced by a factor ranging from 2.8 to 15.5 in comparison to 1.1 to 6 for lateral confinement).

In this microcavity, previous studies have evidenced that the evanescent field is spread over two maxima of electromagnetic field.[43] We observe in Figure 3(b) that *S. epidermidis* and *E. coli* interact with one maximum of the field at a time (*S. epidermidis* stays on one while *E. coli* keeps switching from one maxima to another). This is allowed by their reduced size compared to the size order of the field maxima of the cavity. The flagella (*E. coli* and *B.*

This manuscript was accepted by Appl. Phys. Lett. Click here to see the version of record.

subtilis) seem to induce a larger displacement in the trap and the ability to interact with several maxima of the field. This behavior is consistent with the increased motility of the flagellated bacteria and with the shape of the electromagnetic field in the microcavity.

Bacterium	Confinement Factor $\frac{L_B \cdot l_B}{L_T \cdot l_T}$	Transversal confinement ratio (l_B/l_T)	Lateral confinement ratio (L_B/L_T)
S. epidermidis	57	9.5	6
E. coli	30.6	15.5	2
B. subtilis	3.2	2.8	1.1

Table 1. Numerical analysis of the spatial behavior of trapped and free bacteria. The transversal direction is parallel to the y axis and the lateral one is parallel to the x axis.

In Table 1, more details about confinement are shown. It highlights a stronger effect of the trap on *S. epidermidis* and *E. coli*, than on *B. subtilis* (confinement factors are 57, 30.6 and 3.2 respectively). This table also outlines a more effective confinement along transversal axis than along lateral one. For *S. epidermidis* lateral and transversal confinement are of the same order of magnitude, which can be linked to the spherical shape of the bacterium. On the other hand, for *E. coli* and *B. subtilis* the transversal confinement prevails. It is consistent with the behavior of the bacteria in the trap: they align with the structure, with their longer dimension parallel to the cavity. From this it is inferred that the lateral and transversal contributions provide information on the shape of the object and its symmetry. The size and shape of *B. subtilis* induce only transversal confinement (lateral confinement of 1.1), which explains the low effectiveness of the trap on that bacterium (confinement factor of 3.2) in accordance with experimental results (trapping duration under 10 minutes against more than 1 hour for *S. epidermidis* and *E. coli*). Finally, each type amongst the three investigated bacteria species

This manuscript was accepted by Appl. Phys. Lett. Click here to see the version of record.

possess a very distinct spatial signature, which is linked to their size, shape (symmetry) and flagella.

In parallel, monitoring the optical signal transmitted through the cavity (Figure 4) enables an accurate detection of the trapping effectiveness: we observe high frequency oscillations and intensity drop of about 20% when a bacterium is trapped (Figure 4(a)).

On Figure 4(b) the temporal variation of the optical signal transmitted through the microcavity during the trapping of the three kinds of bacteria is shown. It is compared to the signal detected in the same conditions without trapping. Because the amplitude is the most relevant criterion to discriminate these curves, we calculate the histogram function of the transmitted signal (Figure 4(c)). Its characteristic elements are the full width at half maximum (FWHM) and the probability to have each intensity value. *E. coli* is characterized by a FWHM at least twice larger than the two other bacteria which can be linked to its large lateral displacement in the trap (Figure 3(b, blue curve)). On the contrary, *S. epidermidis* histogram function has a very low FWHM which highlights the unique position of equilibrium for the bacterium (high probability for one intensity value), matching with one field maximum (Figure 3(b, orange curve)). Finally, the optical signal transmitted through the adapted SOI microcavity is self-consistent for bacteria discrimination in this example. This result is reproducible, as shown Figure 4(d) on which the average FWHM and the standard deviation are represented for each type of bacterium (measurements made on four different trapping for each type of bacterium).

We highlighted here that amplitude is a relevant criterion to differentiate the optical signal transmitted through the microcavity, in which the substantial part of the information is located below 15 Hz. It provides information on the maximum and minimum intensity values of the signal shown in Figure 1 and Figure 4. On Figure 5, these Imax and Imin values are represented on the resonance peak of the microcavity, at the injected wavelength. If we

This manuscript was accepted by Appl. Phys. Lett. Click here to see the version of record.

consider that the quality factor remains constant during the trapping (low change of optical index when the microcavity environment is water or bacteria), it allows the calculation of the redshift in the resonance wavelength between the two extreme positions of the bacteria in the trap (from the trap center (Imin) to its edge (Imax)). This redshift is characteristic to bacterium phenotype, as represented Figure 5(b1): its value ranges from 0.20 nm for S. epidermidis to 0.30 nm for *E. coli*. Each colored peak represents the resonant mode available according to the type of trapped bacterium. By projecting these curves on the resonance peak of the optical trapping structure we are able to assign a specific area of the peak to each type of bacterium (Figure 5(b2)) and used it to discriminate them.

Finally, the two methods of characterization (spatial and temporal) are consistent with each other: the displacement of *E. coli* on the two evanescent field maxima can be linked to the large amplitude of its trapping signal and the higher value of the FWHM of its histogram function. *S. epidermidis* oscillates close to its equilibrium position (one field maximum), matching to one transmitted intensity value of highest probability.

In this paper we show that planktonic single cell bacterium can by trapped by the evanescent field of a properly tuned microcavity. Both spatial (Brownian and partially-trapped motions) and temporal (optical transmission measurement) methods are relevant to finely study the bacterium behavior within the trap. The spatial signature demonstrates that morphological properties of bacteria (size, shape and presence of flagella) can be identified through the confinement factor parameter. The temporal signature acquired after the analysis of the fluctuations in the optical transmitted signal over time during bacteria trapping allows us to identify bacteria phenotypes. Compared to the spatial characterization, the temporal method requires only cavity transmission measurements. Thus, this promising label-free technic that can be performed in a much more compact way, with a smaller footprint, in a device scheme

might be suitable to reduce cost in fast analysis device. In the future we plan to extend this study to a larger number of bacteria, with different shapes, sizes and overall properties.

Supplementary material

A clip is provided in the supplementary information. It shows the waveguide which leads light into the microcavity. The optical structure is surrounded by *diplococci* of *Staphylococcus epidermidis* swimming in water and we can see that one is trapped and interacts with the electromagnetic field of the microcavity. This clip illustrates the spatial method of analysis of the trapping described in this paper: on every image we track the position of trapped and free bacteria which leads to the construction of their trajectories.

Acknowledgement

The authors would like to express their gratitude to Pascal Gentile and Christophe Pin for imaging and preparation of bacteria. A thank you is also extended to Julien Cordeiro for his blender images and to Patricia Laurent for the bacteria samples preparation. We would also acknowledge the technical group in the "Plateforme Technologique Amont" of Grenoble for their help in nanofabrication.

This manuscript was accepted by Appl. Phys. Lett. Click here to see the version of record.

Figure captions:

FIG. 1. Redshift of the microcavity resonance wavelength in presence of a bacterium above it. **(a)** High quality factor structure which is ideal for detection of the target object with no trapping of bacteria. **(b)** Intermediate quality factor structure, ideal for bacteria trapping and analysis.

FIG. 2. (a) SEM image of the single microcavity used for all the experiments. **(b)** Trapping set-up: fluidic system on a 1D PhC, light injected in the optical structure with a polarized fiber and recorded on structure output (TEMPORAL). Second trapping analysis by microscopy column above the cavity (SPATIAL). The measurements related to E. coli are shown in blue and those associated with S. epidermidis are shown in orange, **(c)** SEM images of the under study bacteria: **(1)** *diplococcus of Staphylococcus epidermidis*, **(2)** *Escherichia coli* and **(3)** aggregate of *Bacillus subtilis*.

FIG. 3. (a) Brownian motion of a *diplococcus* of *S. epidermidis* (orange curve), an *E. coli* cell (blue curve) and a *B. subtilis* aggregate (red curve) during 50 seconds, tracking of bacteria center. **(b)** Trapped trajectories of *S. epidermidis diplococcus* (orange curve), *E. coli* (blue curve) and *B. subtilis* (red curve) during 50 seconds. Tracking of bacteria center for *S. epidermidis* and *E. coli*, tracking at left edge (L), center (C) and right edge (R) for *B. subtilis*.

FIG. 4. (a) 20% drop in the optical signal transmitted through the microcavity, start of bacteria trapping. **(b)** Example of intensity transmitted through the microcavity during 10 seconds of trapping for the bacteria *S. epidermidis diplococcus* (orange), *E. coli* (blue), *B. subtilis* aggregate (red) and with no bacteria trapped (in bacteria and water medium) (black). **(c)** Histogram function of the transmitted optical signal. **(d)** Average FWHM for each type of

bacterium (measurements on four different trapping by type of bacterium). Standard deviation is also represented and shows three distinct signatures with no overlap.

FIG. 5. (a) Experimental measurements, resonance peak of the optical structure used to trap bacteria (in black) and lorentzian fit of this curve (in grey), using Fityk[45] (curve fitting and peak fitting software). **(b) (1)** Redshift in the microcavity resonance wavelength in presence of a *diplococcus* of *S. epidermidis* (orange curve), an aggregate of *B. subtilis* (red curve) and an *E. coli* cell (blue curve) above the optical trap. **(2)** Representation of the redshift in the resonance curve, delineated areas for each type of trapped bacterium. These curves were obtained by a lorentzian fit to experimental curves, at the right scale.

References

[1] A. Ashkin and J.M. Dziedzic, Science **235**, 1517 (1987).

[2] J. Enger, M. Goksör, K. Ramser, P. Hagberg, and D. Hanstorp, Lab Chip **4**, 196 (2004).

[3] K. Konig, H. Liang, M.W. Berns, and B.J. Tromberg, Opt. Lett. **21**, 1090 (1996).

[4] Y. Liu, G.J. Sonek, M.W. Berns, and B.J. Tromberg, Biophys. J. **71**, 2158 (1996).

[5] K.C. Neuman, E.H. Chadd, G.F. Liou, K. Bergman, and S.M. Block, Biophys. J. **77**, 2856 (1999).

[6] M. Ericsson, D. Hanstorp, P. Hagberg, and J. Enger, J. Bacteriol. **182**, 5551 (2000).

[7] M.B. Rasmussen, L.B. Oddershede, and H. Siegumfeldt, Appl. Environ. Microbiol. **74**, 2441 (2008).

[8] S. Mandal, J.M. Goddard, and D. Erickson, Lab Chip **9**, 2924 (2009).

[9] S. Lin and K.B. Crozier, ACS Nano 7, 1725 (2013).

[10] M.R. Lee and P.M. Fauchet, Opt. Express **15**, 4530 (2007).

[11] S. Pal, P.M. Fauchet, and B.L. Miller, Anal. Chem. **84**, 8900 (2012).

[12] F. Vollmer, D. Braun, A. Libchaber, M. Khoshsima, I. Teraoka, and S. Arnold, Appl. Phys. Lett. **80**, 4057 (2002).

[13] P. Kang, P. Schein, X. Serey, D. O'Dell, and D. Erickson, Sci. Rep. **5**, 12087 (2015).

[14] F. Vollmer, S. Arnold, and D. Keng, Proc. Natl. Acad. Sci. U. S. A. **105**, 20701 (2008).

[15] T. van Leest and J. Caro, Lab Chip **13**, 4358 (2013).

[16] S. Chan, S.R. Horner, P.M. Fauchet, and B.L. Miller, J. Am. Chem. Soc. **123**, 11797 (2001).

[17] P.B. Deotare, M.W. McCutcheon, I.W. Frank, M. Khan, and M. Lončar, Appl. Phys. Lett. **94**, 1 (2009).

[18] M.W. McCutcheon and M. Loncar, Opt. Express **16**, 19136 (2008).

[19] M. Galli, D. Bajoni, F. Marabelli, L.C. Andreani, L. Pavesi, and G. Pucker, Phys. Rev. B **69**,

115107 (2004).

[20] M. Notomi, E. Kuramochi, and H. Taniyama, Conf. Proc. - Lasers Electro-Optics Soc. Annu.

Meet. **16**, 689 (2008).

[21] Y. Akahane, T. Asano, B. Song, and S. Noda, Nature **425**, 944 (2003).

[22] Z. Zhang and M. Qiu, Opt. Express **12**, 3988 (2004).

[23] J.B. Jager, V. Calvo, E. Delamadeleine, E. Hadji, P. Noé, T. Ricart, D. Bucci, and A. Morand,

Appl. Phys. Lett. **99**, 2014 (2011).

[24] T.J. Kippenberg, S.M. Spillane, and K.J. Vahala, Appl. Phys. Lett. **85**, 6113 (2004).

[25] D.K. Armani, T.J. Kippenberg, S.M. Spillane and K.J.Vahala, **421**, 925 (2003).

[26] T. Baehr-Jones, M. Hochberg, C. Walker, and A. Scherer, Appl. Phys. Lett. **85**, 3346 (2004).

[27] I. Grudinin, A. Savchenkov, A. Matsko, D. Strekalov, V. Ilchenko, and L. Maleki, IQEC,

Int. Quantum Electron. Conf. Proc. **2005**, 380 (2005).

[28] M.L. Gorodetsky and V.S. Ilchenko, J. Opt. Soc. Am. B **16**, 147 (1999).

[29] L. Collot, V. Lefèvre-Seguin, M. Brune, J.M. Raimond, and S. Haroche, Europhys. Lett. **23**,

327 (2007).

[30] A. Rahmani and P.C. Chaumet, Opt. Express **14**, 6353 (2006).

[31] C. Pin, B. Cluzel, C. Renaut, D. Peyrade, E. Picard, E. Hadji, and F. De Fornel, Appl. Phys. Lett. **105**, 2012 (2014).

[32] C. Renaut, B. Cluzel, J. Dellinger, L. Lalouat, E. Picard, D. Peyrade, E. Hadji, and F. de Fornel, Sci. Rep. **3**, 2290 (2013).

[33] S. Mandal, X. Serey, and D. Erickson, Nano Lett. **10**, 99 (2010).

[34] N. Descharmes, U.P. Dharanipathy, Z. Diao, M. Tonin, and R. Houdre, Lab Chip **13**, 3268 (2013).

[35] S. Lin, E. Schonbrun, and K. Crozier, Nano Lett. **10**, 2408 (2010).

[36] H. Cai and A.W. Poon, Opt. Lett. **35**, 2855 (2010).

[37] M.S. Luchansky and R.C. Bailey, Anal. Chem. **84**, 793 (2012).

[38] F. Vollmer, L. Yang, and S. Fainman, Nanophotonics **1**, 267 (2012).

[39] P. Velha, E. Picard, T. Charvolin, E. Hadji, J.C. Rodier, P. Lalanne, and D. Peyrade, Opt. Express **15**, 16090 (2007).

[40] J. Schindelin, I. Arganda-Carreras, E. Frise, V. Kaynig, M. Longair, T. Pietzsch, S. Preibisch, C. Rueden, S. Saalfeld, B. Schmid, J.-Y. Tinevez, D.J. White, V. Hartenstein, K. Eliceiri, P. Tomancak, and A. Cardona, Nat. Methods **9**, 676 (2012).

[41] J.B. Bateman, J. Wagman, and E.L. Carstensen, Kolloid-Zeitschrift Zeitschrift für Polym. **208**, 44 (1966).

[42] C. Renaut, J. Dellinger, B. Cluzel, T. Honegger, D. Peyrade, E. Picard, F. De Fornel, and E. Hadji, Appl. Phys. Lett. **100**, 1 (2012).

[43] C. Pin, B. Cluzel, C. Renaut, E. Picard, D. Peyrade, E. Hadji, and F. De Fornel, ACS Photonics **2**, 1410 (2015).

[44] J.M. Willey, L. M. Sherwood and C. J. Woolverton, Prescott Harley and Klein's Microbiology Seventh Edition (Mc Graw Hill, New York, 2008).

[45] M. Wojdyr, J. Appl. Cryst. 43, 1126–1128 (2010).

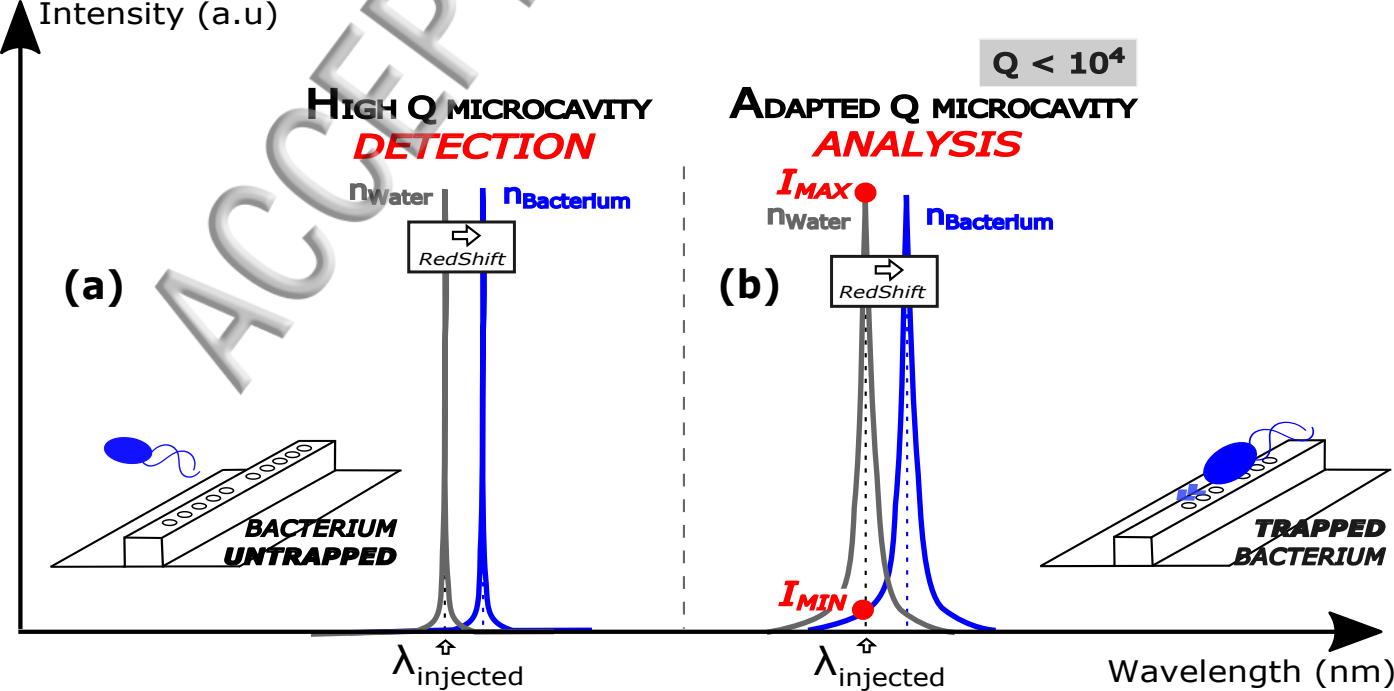
Intensity (a.u)
HIGH Q MICROCAVITY
DETECTION
ADAPTED Q MICROCAVITY
ANALYSIS
Q < 10⁴
(a)
(b)
n Water
n Bacterium
RedShift
I MAX
I MIN
BACTERIUM
UNTRAPPED
TRAPPED
BACTERIUM
λ injected
λ injected
Wavelength (nm)

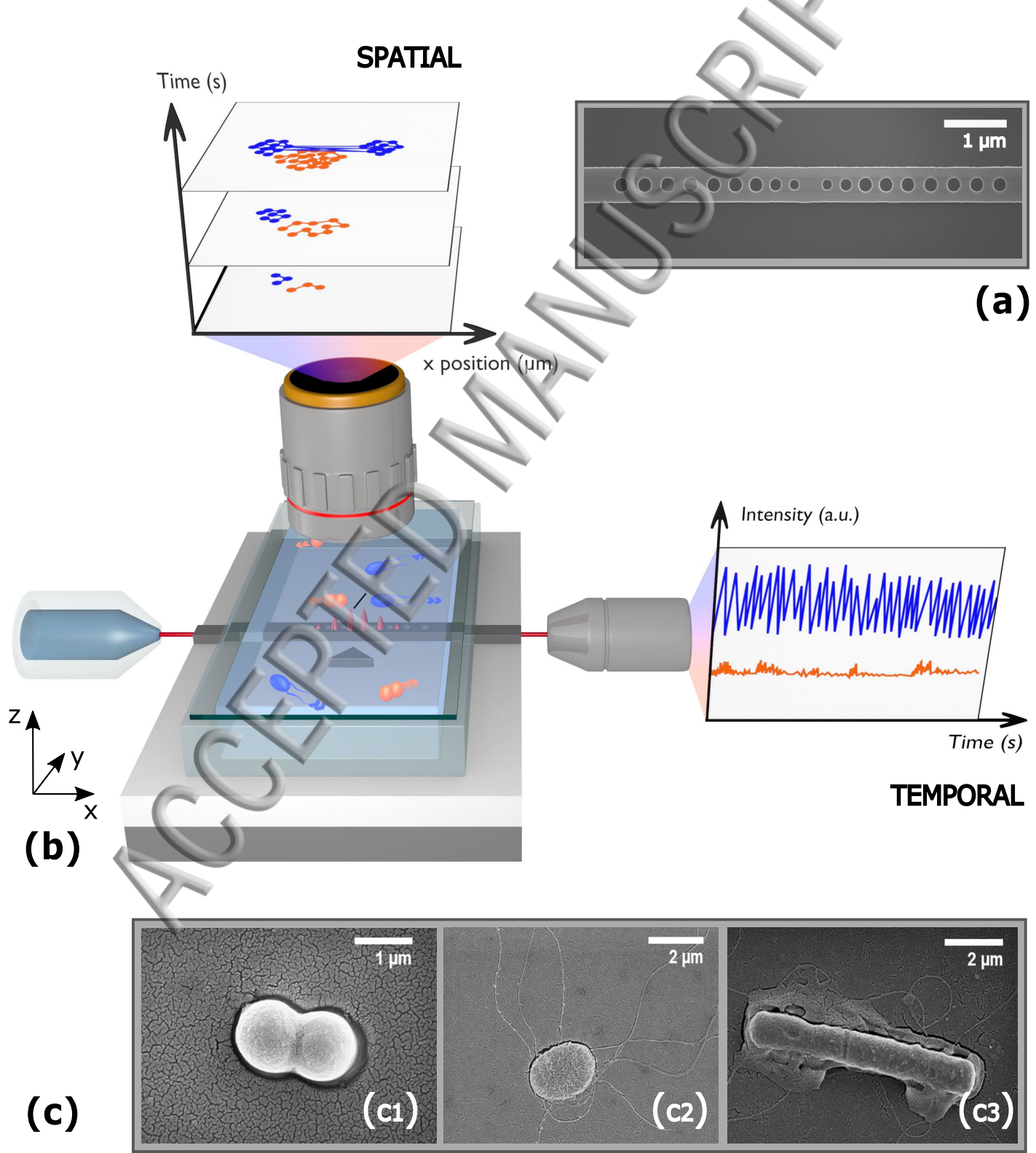

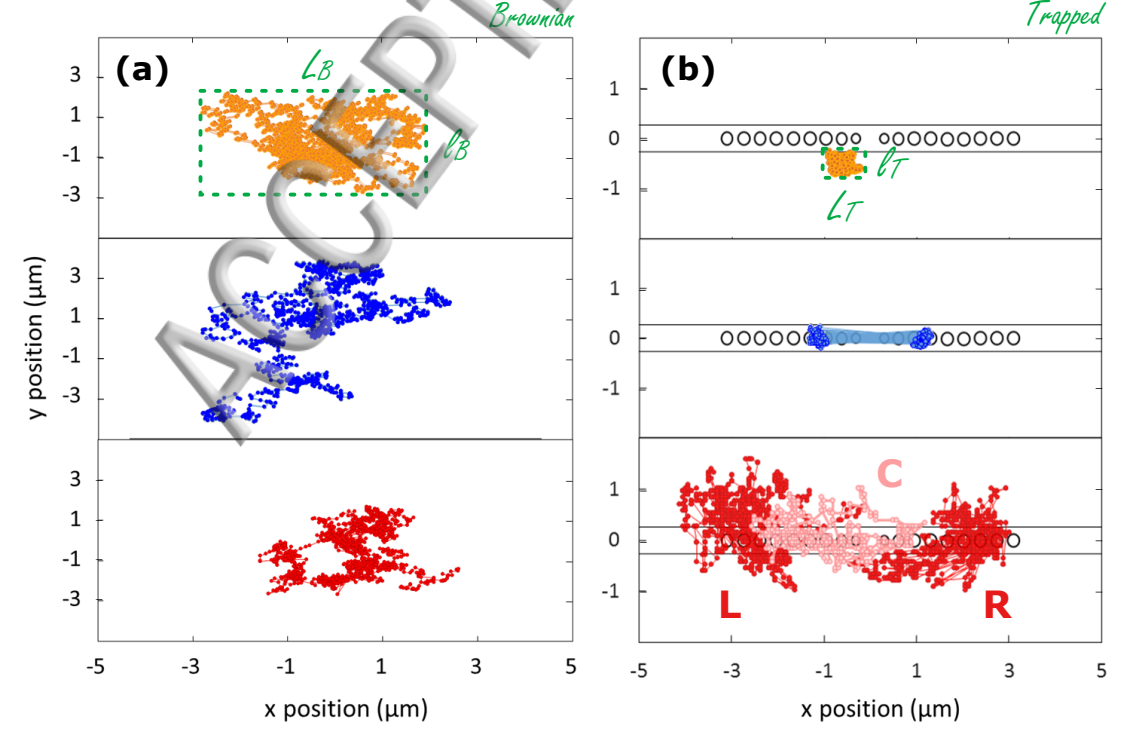
Brownian
Trapped
(a)
(b)
L_B
l_B
l_T
L_T
C
L
R
y position (μm)
x position (μm)
x position (μm)

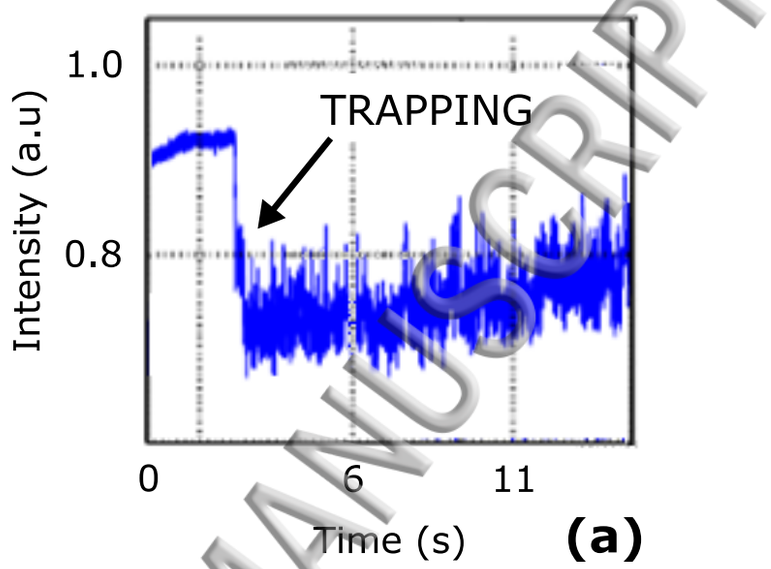

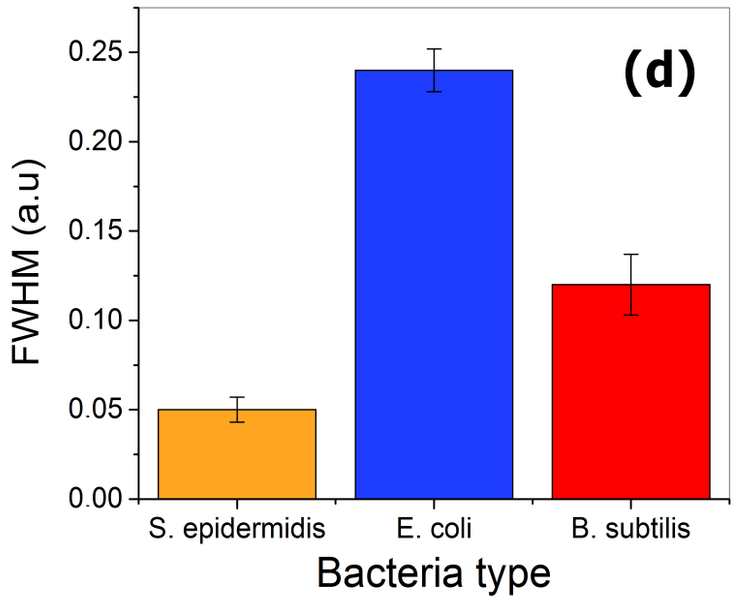

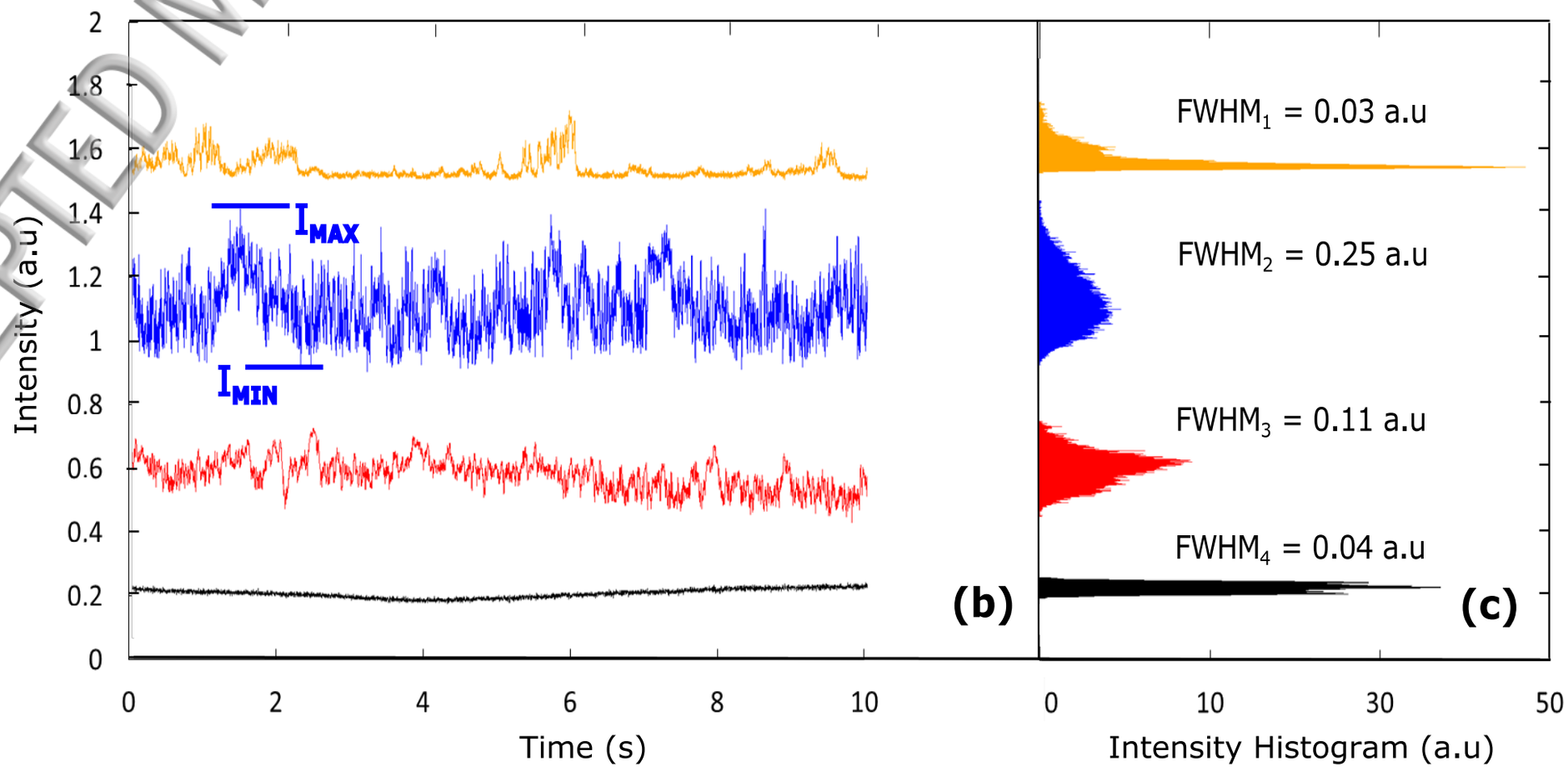

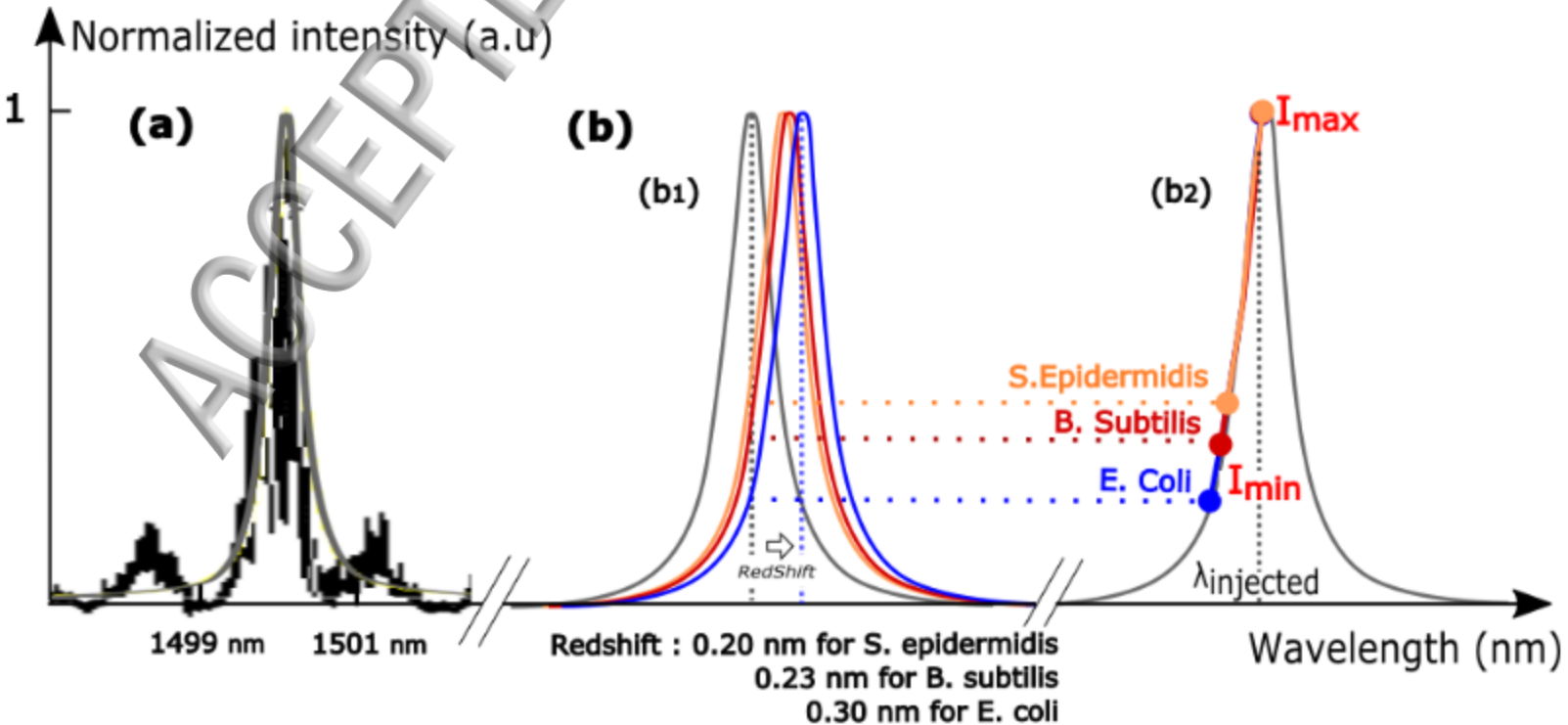
Normalized intensity (a.u)
1
(a)
(b)
(b1)
(b2)
Imax
S.Epidermidis
B. Subtilis
E. Coli
Imin
RedShift
λinjected
1499 nm
1501 nm
Redshift : 0.20 nm for S. epidermidis
0.23 nm for B. subtilis
0.30 nm for E. coli
Wavelength (nm)